Available online at www.sciencedirect.com
ScienceDirect
Carbohydrate Research 341 (2006) 2565–2574
Carbohydrate RESEARCH

An investigation of the pyranose ring interconversion path of α-L-idose calculated using density functional theory

Youji Kurihara* and Kazuyoshi Ueda*

Department of Advanced Materials Chemistry, Graduate School of Engineering, Yokohama National University, 79-5 Tokiwadai, Hodogaya-Ku, Yokohama 240-8501, Japan

Received 15 March 2006; received in revised form 4 July 2006; accepted 18 July 2006
Available online 22 August 2006

Abstract—The interconversion pathways of the pyranose ring conformation of α-L-idose from a $^4C_1$ chair to other conformations were investigated using density functional calculations. From these calculations, four different ring interconversion paths and their transition state structures from the $^4C_1$ chair to other conformations, such as $B_{3,O}$, and $^1S_3$, were obtained. These four transition-state conformations cover four possible combinations of the network patterns of the hydroxyl group hydrogen bonds (clockwise and counterclockwise) and the conformations of the primary alcohol group (*tg* and *gg*). The optimized conformations, transition states, and their intrinsic reaction coordinates (IRC) were all calculated at the B3LYP/6-31G** level. The energy differences among the structures obtained were evaluated at the B3LYP/6-311++G** level. The optimized conformations indicate that the conformers of $^4C_1$, ^2S_O, and $B_{3,O}$ have similar energies, while $^1S_3$ has a higher energy than the others. The comparison of the four transition states and their ring interconversion paths, which were confirmed using the IRC calculation, suggests that the most plausible ring interconversion of the α-L-idopyranose ring occurs between $^4C_1$ and $B_{3,O}$ through the E_3 envelope, which involves a 5.21 kcal/mol energy barrier.

Keywords: Idopyranose conformation; Ab initio calculation; Transition state; Ring puckering

1. Introduction

The ring interconversion paths and the transition-state structures of α-L-idopyranose from the $^4C_1$ chair to other conformations were investigated using density functional theory (B3LYP) with the 6-31G** basis set. In the D-series, the $^4C_1$ chair is usually considered the most stable conformation. In fact, the preferential existence of the $^4C_1$ conformation has been identified for D-allose, D-glucose, D-mannose, D-gulose, D-galactose, and D-talose using NMR spectroscopy.[1–3] In contrast, for α-D-altrose, equilibrium of the coexisting $^4C_1$ and $^1C_4$ conformations was found using NMR spectroscopy.[2,3] Moreover, α-D-idose was found by NMR spectroscopy to have the $^OS_2$ skew boat (in the L-series, ^2S_O) conformation, in addition to the $^4C_1$ and $^1C_4$ conformations.[2–4] The conformation of α-idose in the L-series is especially interesting because it is observed in biological molecules. Typical examples include the glycosaminoglycans heparin and heparan sulfate, which contain α-L-idose as a constituent in the form of a uronic acid. Therefore, the ring conformation of idopyranose derivatives has long been the subject of research.

The important ring conformations of α-L-iduronic acid are the $^1C_4$ and $^4C_1$ chairs, and the ^2S_O skew boat. These conformations have been investigated precisely using many methods, including NMR spectroscopy,[5–10] X-ray diffraction,[11–13] molecular dynamics,[14–19] and quantum chemistry.[20–22] The three conformers equilibrate with each other in solution, and conformational flexibility is believed to play an important role in their

* Corresponding authors. Tel./fax: +81 45 339 3945; e-mail: k-ueda@ynu.ac.jp

0008-6215/$ - see front matter © 2006 Elsevier Ltd. All rights reserved.
doi:10.1016/j.carres.2006.07.015

biological activities.[23,24] However, the conformational preferences and their flexibility are still debated. In particular, the energy barrier and interconversion path between these conformers have not been investigated fully.

Ragazzi et al. calculated the interconversion of (methyl 4-*O*-methyl-2-*O*-sulfate-α-L-idopyranoside) uronic acid (DMIS) between $^{2}S_{O}$, $^{4}C_{1}$, and $^{1}C_{4}$ using a molecular mechanics calculation.[14] However, they constrained one of the ring-puckering parameters defined by Cremer and Pople.[25] Ernst et al. presented a graphical procedure in terms of stereochemically accessible iduronate ring conformations.[17] They suggested that the most likely interconversion path goes from $^{4}C_{1}$ to a region between $^{2}S_{O}$ and $^{1}S_{3}$, whereas interconversion from $^{1}C_{4}$ goes to a region between $^{O}S_{2}$ and $^{3}S_{1}$. However, they did not calculate an actual path or the conformation of the transition state (TS). The purpose of their procedure was to exclude inaccessible conformations and not to predict the obvious interconversion path. Recently, Ionescu et al. investigated the conformational potential energy surface of the glucopyranose ring in a precise manner.[26] They introduced a new quantitative expression to characterize the pyranose ring conformation and surveyed the conformations along the selected ring interconversion paths by constraining their derived dihedral parameters. Since all of these works placed some constraints on the conformation, the paths obtained might not represent the optimum ring interconversion path along the reaction coordinates. No transition states of ring interconversion obtained with no constraints on the conformation have been obtained.

In general, it is difficult to determine an interconversion path for sugar rings. In this study, we investigated the interconversion paths among idopyranose ring conformations using α-L-idopyranose as a basic model for idopyranose derivatives. We focused on the ring interconversion from the $^{4}C_{1}$ chair structure to the boat and skewed ring conformations, and obtained the transition-state conformers for these interconversion paths under conditions with no constraints on the conformation using the ab initio calculation. The results showed that the most plausible ring interconversion path connects $^{4}C_{1}$ and $B_{3,O}$ through the transition-state conformation of the E_{3} envelope with a barrier of 5.21 kcal/mol. The conformation of the transition state was confirmed using intrinsic reaction coordinate (IRC) calculations.

2. Computational details

We focused on the $^{4}C_{1}$ chair, $^{2}S_{O}$ skew boat, $B_{3,O}$ boat, and $^{1}S_{3}$ skew boat conformations of α-L-idopyranose because Ernst et al. proposed that the most likely interconversion path from $^{4}C_{1}$ goes to a region between $^{2}S_{O}$ and $^{1}S_{3}$.[17] The nomenclature for α-L-idopyranose used in this study is shown in Figure 1. This molecule has six rotational exocyclic bonds, which include the five C–O bonds of the hydroxyl groups and the C-5–C-6 bond of the hydroxymethyl group. The six rotations can generate $3^{6} = 729$ different conformers. In order to obtain the optimized conformation for each $^{4}C_{1}$, $^{2}S_{O}$, $B_{3,O}$, and $^{1}S_{3}$ ring conformation, all 729 different conformers of α-L-idopyranose for each ring conformation were initially optimized with no constraints using the Hartree–Fock method with the 4-31G basis set. Then, some of the optimized conformers that lay within 2.5 kcal/mol above the lowest energy for each $^{4}C_{1}$, $^{2}S_{O}$, $B_{3,O}$, or $^{1}S_{3}$ ring conformation were again fully optimized at the B3LYP/6-31G** level. The results of this density functional level were comparable to those of the MP2 calculation of HF theory.[27,28] The optimization at the B3LYP/6-31G** resulted in the various conformations of hydroxyl and hydroxymethyl groups for each $^{4}C_{1}$, $^{2}S_{O}$, $B_{3,O}$, or $^{1}S_{3}$. We evaluated the energies of these conformations in each ring type at the B3LYP/6-311++G** and selected the optimized $^{4}C_{1}$, $^{2}S_{O}$, $B_{3,O}$, and $^{1}S_{3}$ geometries, which had the lowest energy in each ring type. Csonka investigated the optimal selection of the basis set for carbohydrates.[21] His results showed that the best energy was obtained when B3LYP/6-311+G(d,p) or B3LYP/6-311++G(d,p) was selected after the geometry was optimized at B3LYP/6-31G* or B3LYP/6-31+G*. Our condition is almost similar to Csonka's selection of basis set.

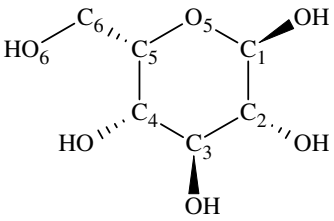

Figure 1. Structure and numbering for α-L-idopyranose.

Transition-state conformers of the ring interconversion paths from the $^{4}C_{1}$ chair to the skew and boat conformations were explored at the B3LYP/6-31G** level. The initial guess of the TS geometries were the E_{3} envelope conformation with the combination of the orientation pattern of the hydroxymethyl and hydroxyl groups (*tg-r*, *gg-r*, *tg-c*, and *gg-c*), because Ernst et al. predicted the ring oxygen participates in the interconversion process. Then, the intrinsic reaction coordinates were calculated to confirm whether the transition-state conformers obtained were stationary states of the ring interconversion paths. The energy differences between the transition-state conformers were also calculated at the B3LYP/6-311++G** level. All calculations were performed using the program GAUSSIAN03.[29] The threshold value of both the optimization and the tran-

sition-state calculations were the default in GAUSSIAN03 program.

3. Results and discussion

3.1. Optimized conformation of ring conformers

The optimized conformations of $^4C_1$, ^2S_O, $B_{3,O}$, and $^1S_3$ calculated using the density functional theory B3LYP/6-311++G**//B3LYP/6-31G** are shown in Figure 2a–d. These conformations were abbreviated by adding (OPT) after the name of the ring conformation. The conformations of $^4C_1$ (OPT), ^2S_O (OPT), and $^1S_3$ (OPT) formed a counterclockwise (*r*) hydrogen-bond network of hydroxyl groups, whereas $B_{3,O}$ (OPT) formed a clockwise (*c*) orientation, except for the hydroxyl groups on the C-1 atoms. These hydrogen-bond networks were abbreviated in combination with the ring conformations as $^4C_1$-*r* (OPT), ^2S_O-*r* (OPT), $B_{3,O}$-*c* (OPT), and $^1S_3$-*r* (OPT), respectively. Furthermore, the primary alcohol group orientations of these $^4C_1$-*r* (OPT), ^2S_O-*r* (OPT), $B_{3,O}$-*c* (OPT), and $^1S_3$-*r* (OPT) were found to have *tg*, *tg*, *gg*, and *tg* conformations,

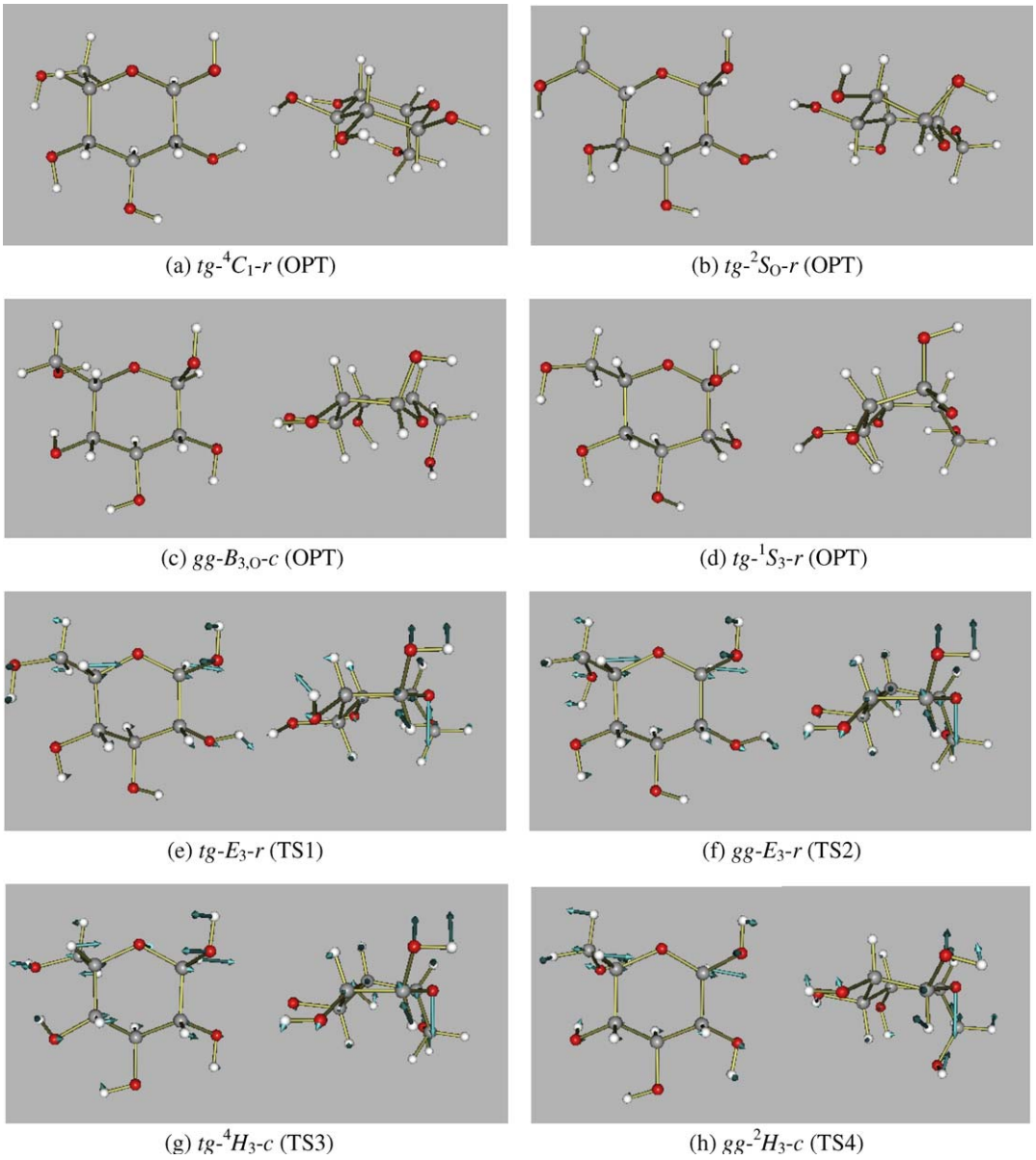

Figure 2. Top and side views of the structures calculated at the B3LYP/6-31G** level. The optimized structures of $^4C_1$, ^2S_O, $B_{3,O}$ and $^1S_3$ are shown in (a)–(d). The four transition-state conformations obtained from TS1 to TS4 are shown in (e)–(h), where the arrows (blue) indicate the direction of the imaginary vibrational mode at the transition state. The conformations at the termination of the IRC calculations on both sides are shown in (i) chair side from TS1, (j) skew side from TS1, (k) chair side from TS2, (l) skew side from TS2, (m) chair side from TS3, (n) skew side from TS3, (o) chair side from TS4, and (p) skew side from TS4.

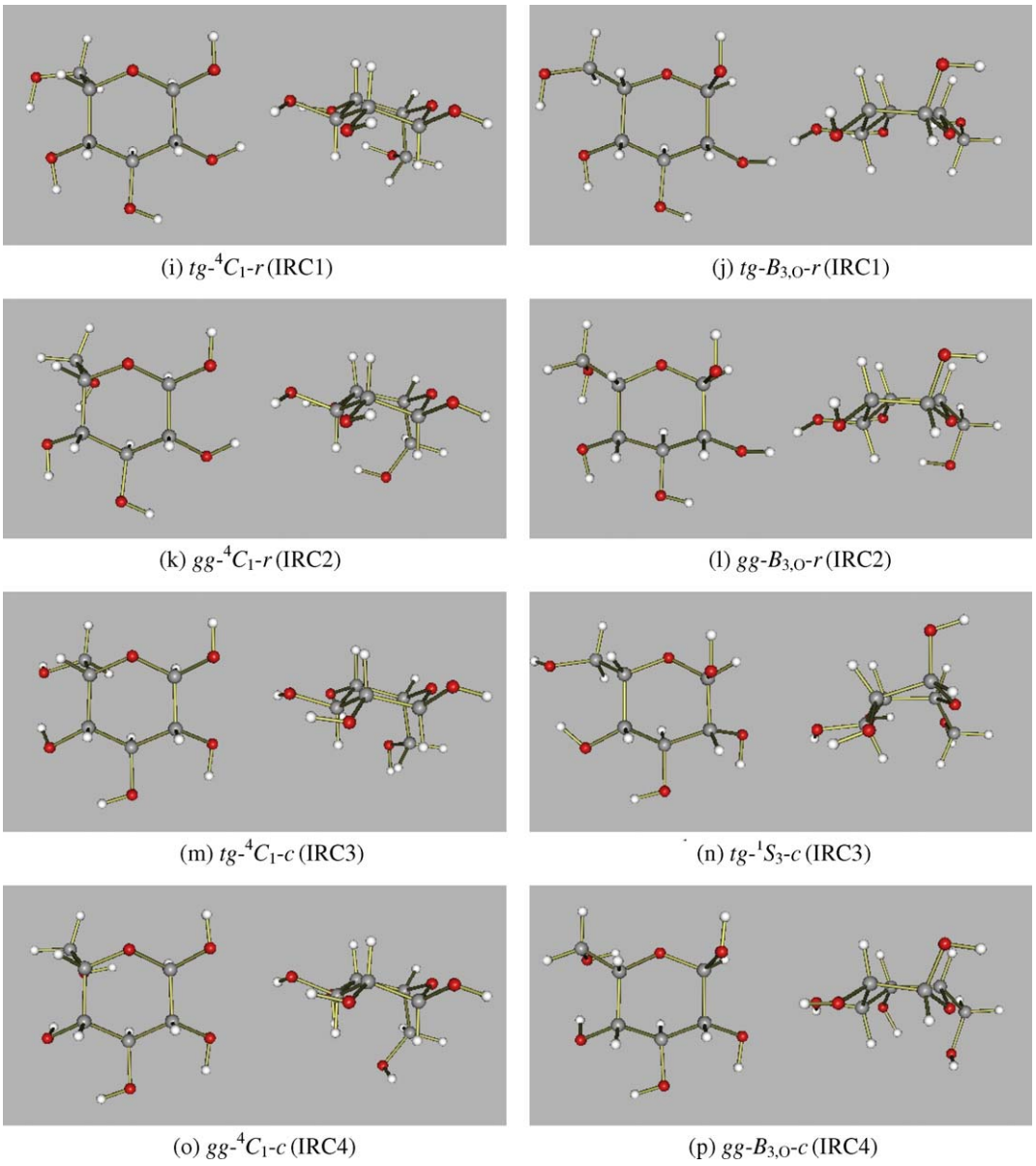

Figure 2. (*continued*)

respectively. The conformational parameters of these conformations are summarized in Table 1. Only *gg*-$B_{3,O}$-*c* (OPT) had different side-chain orientations.

The energy differences for these optimization structures calculated at the B3LYP/6-311++G** level are shown in Figure 3. It is apparent that *tg*-$^4C_1$-*r* (OPT) has the most stable conformation. The *tg*-^2S_O-*r* (OPT) and *gg*-$B_{3,O}$-*c* (OPT) conformations were within about 1 kcal/mol of the value for *tg*-$^4C_1$-*r* (OPT). From an energy perspective, one can state that these conformers have similar stability. In contrast, the energy of the *tg*-$^1S_3$-*r* (OPT) conformation was 3.8 kcal/mol higher than that of *tg*-$^4C_1$-*r* (OPT). Note that our calculation suggests that the $B_{3,O}$ conformation is favored over the ^2S_O conformation, although the ^2S_O conformation is usually considered the most stable skewed conformation of α-L-idopyranose.[14,17]

3.2. Transition states of ring interconversion

The transition state structures of the ring interconversion paths from $^4C_1$ to the boat and skew conformations were explored at the B3LYP/6-31G** level. We obtained four transition-state conformers, labeled TS1 to TS4. These conformers are shown in Figure 2e–h. The analysis of these conformers indicates that they correspond to *tg*-E_3-*r*, *gg*-E_3-*r*, *tg*-$^4H_3$-*c*, and *gg*-$^2H_3$-*c*. The details of the conformational parameters of these transition-state conformations are summarized in Table 1. Each transition state was confirmed to have one imaginary

Table 1. Internal coordinates of the optimized, TS geometries calculated at the B3LYP/6-31G** for α-L-idopyranose

	OPT				TS1	TS2	TS3	TS4
	tg-$^4C_1$-*r*	*tg*-^2S_O-*r*	*gg*-$B_{3,O}$-*c*	*tg*-$^1S_3$-*r*	*tg*-E_3-*r*	*gg*-E_3-*r*	*tg*-$^4H_3$-*c*	*gg*-$^2H_3$-*c*
Bond length (Å)								
C1–C2	1.528	1.539	1.541	1.547	1.530	1.527	1.536	1.523
C2–C3	1.521	1.523	1.522	1.528	1.514	1.514	1.518	1.518
C3–C4	1.527	1.527	1.529	1.524	1.522	1.523	1.526	1.524
C4–C5	1.542	1.550	1.562	1.553	1.548	1.550	1.540	1.557
C5–O5	1.438	1.438	1.444	1.447	1.444	1.442	1.431	1.440
O5–C1	1.422	1.413	1.426	1.415	1.413	1.411	1.435	1.432
O1–C1	1.397	1.411	1.404	1.408	1.410	1.412	1.401	1.393
O2–C2	1.420	1.425	1.418	1.425	1.423	1.422	1.419	1.414
O3–C3	1.423	1.418	1.419	1.423	1.421	1.420	1.418	1.420
O4–C4	1.427	1.431	1.425	1.426	1.425	1.430	1.422	1.426
O6–C6	1.414	1.414	1.431	1.412	1.412	1.417	1.434	1.431
C5–C6	1.541	1.532	1.523	1.534	1.540	1.535	1.538	1.528
Bond angle (deg)								
C1–C2–C3	109.1	108.9	109.3	109.7	110.0	109.6	111.9	108.9
C2–C3–C4	110.1	109.6	110.7	110.2	107.4	107.6	108.3	110.6
C3–C4–C5	111.5	110.1	109.8	109.3	111.4	111.9	109.6	112.7
C4–C5–O5	109.1	110.8	110.7	110.8	113.8	114.4	113.0	115.0
C5–O5–C1	115.9	114.3	115.0	115.7	126.4	126.2	125.8	126.1
O5–C1–C2	110.7	112.3	112.3	112.1	115.8	115.4	117.1	114.2
O1–C1–C2	107.0	106.9	108.0	107.2	105.8	105.8	106.7	108.0
O2–C2–C3	107.4	107.3	111.5	110.7	108.0	108.0	111.9	111.2
O3–C3–C4	106.7	108.0	111.2	107.3	106.9	106.8	111.0	110.6
O4–C4–C5	109.4	110.6	115.1	110.0	109.5	109.5	114.4	112.8
O6–C6–C5	111.3	111.5	110.3	112.0	112.5	113.5	108.3	113.0
C6–C5–O5	113.1	106.6	104.5	105.5	105.8	106.6	105.6	108.4
Dihedral angle (deg)								
C1–C2–C3–C4	−55.5	−64.3	−59.8	−42.2	−63.9	−65.4	−55.0	−63.4
C2–C3–C4–C5	54.5	40.3	50.1	64.3	85.4	59.1	66.7	53.3
C3–C4–C5–O5	−52.6	20.4	7.1	−23.2	−28.1	−23.0	−43.3	−25.9
C1–O5–C5–C4	56.3	−65.0	−60.0	−39.7	−4.7	−8.2	9.8	10.7
C2–C1–O5–C5	−59.6	40.2	50.5	63.2	2.5	1.6	1.3	−21.6
C3–C2–C1–O5	56.9	23.7	10.2	−18.04	32.4	35.7	21.8	46.4
H1–O1–C1–C2	178.5	178.2	173.4	−179.2	177.0	175.5	174.5	176.5
H2–O2–C2–C3	179.4	−165.7	−49.4	64.5	−171.0	−173.9	−54.2	−47.3
H3–O3–C3–C4	−175.6	−169.5	49.1	−175.4	−166.4	−166.1	41.3	46.0
H4–O4–C4–C5	167.7	176.6	44.0	163.5	167.6	172.3	19.2	60.8
O6–C6–C5–O5	−160.8	176.2	59.9	−166.1	−161.4	75.7	−169.4	78.2
H6–O6–C6–C5	−56.0	−70.2	−54.1	−63.7	−62.9	72.0	−175.9	−66.6
C6–C5–O5–C1	−72.4	171.1	177.9	−163.4	−129.8	−133.1	−115.9	−116.2

frequency. The imaginary frequencies of TS1, TS2, TS3, and TS4 were −110.3, −110.4, −109.3, and −126.2 cm^{-1}, respectively. In all cases, the ring oxygen atoms had the largest amplitudes, as seen in the side view of each figure in Figure 2e–h.

The energies for these transition-state structures were calculated at the B3LYP/6-311++G** level, and the results are shown in Figure 3 according to the energy differences measured from the lowest value of *tg*-$^4C_1$-*r* (OPT). Note that the conformational energies of *tg*-E_3-*r* (TS1) and *gg*-E_3-*r* (TS2) are more stable than those of *tg*-$^4H_3$-*c* (TS3) and *gg*-$^2H_3$-*c* (TS4). Of the four, *tg*-E_3-*r* (TS1) has the most stable conformation.

For all transition states, we performed IRC calculations in the forward and reverse directions at the B3LYP/6-31G** level to determine the ring interconversion path and to confirm the terminal conformation. The IRC calculation from TS1 in one direction reached the $B_{3,O}$ ring conformation, which we abbreviated as *tg*-$B_{3,O}$-*r* (IRC1). A similar calculation from *tg*-E_3-*r* (TS1) in the other direction reached the $^4C_1$ conformation (abbreviated *tg*-$^4C_1$-*r* (IRC1)). These calculations confirmed that E_3 is a transition state that connects the path from $^4C_1$ to $B_{3,O}$. The conformational parameters of these IRC terminal conformations are summarized in Table 2.

The energies for these conformers of *tg*-E_3-*r* (TS1), *tg*-$^4C_1$-*r* (IRC1), and *tg*-$B_{3,O}$-*r* (IRC1) were calculated and the results are shown in Figure 3 as the energy differences measured from *tg*-$^4C_1$-*r* (OPT). The energy of *tg*-$^4C_1$-*r* (IRC1) was only 0.11 kcal/mol higher than that of *tg*-$^4C_1$-*r* (OPT). These two conformers are compared

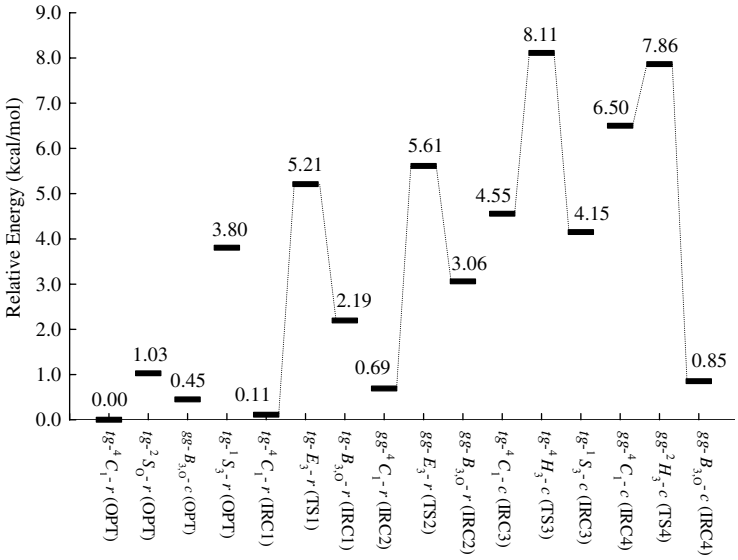

Figure 3. The relative energies of the α-L-idopyranose conformers calculated in this work at the B3LYP/6-311++G**//B3LYP/6-31G** level. The energy of *tg*-$^4C_1$-*r* (OPT) was −687.39841 hartree.

in Figure 2a and i, which show that they have the same *tg*-counterclockwise hydroxyl conformation. These results indicate that the conformations of *tg*-$^4C_1$-*r* (OPT) and *tg*-$^4C_1$-*r* (IRC1) are essentially the same.

In contrast, the energy of *tg*-$B_{3,O}$-*r* (IRC1) was 1.74 kcal/mol higher than that of *gg*-$B_{3,O}$-*c* (OPT). These two conformers are also shown in Figure 2c and j. Note that these conformations have different hydroxyl group orientations. Therefore, *tg*-$B_{3,O}$-*r* (IRC1) must change the hydroxyl conformations again in order to reach the lower conformation of *gg*-$B_{3,O}$-*c* (OPT) in energy. However, the occurrence of such hydroxyl rotation is common in carbohydrates. For example, the hydroxymethyl rotation of glucose in aqueous solution was observed in an NMR experiment and in a molecular dynamics simulation.[30,31] Therefore, rotation of the hydroxyl group of α-L-idopyranose might also frequently occur in solution. These results indicate that the conformational transition of α-L-idopyranose from $^4C_1$ to $B_{3,O}$ via E_3 can be summarized as follows. First, the conformation changes from *tg*-$^4C_1$-*r* to *tg*-E_3-*r* transition state. This is then converted to *tg*-$B_{3,O}$-*r*, and finally, the hydroxyl groups rotate toward *gg*-$B_{3,O}$-*c*.

Next, the path of the ring conformational change via the transition state of *gg*-E_3-*r* (TS2) was investigated using IRC calculations. Although the ring conformation of TS2 had the same E_3 conformation as TS1, the hydroxyl group orientation differed because TS1 had the *tg* conformation, while TS2 had the *gg* conformation. The results of the IRC calculation showed that TS2 was a transition state along the path from *gg*-$^4C_1$-*r* (IRC2) to *gg*-$B_{3,O}$-*r* (IRC2). As shown in Figure 2k and l, the hydroxyl conformations of these two conformers had the same *gg*-counterclockwise orientation, and all the conformers of *gg*-$^4C_1$-*r* (IRC2), *gg*-$B_{3,O}$-*r* (IRC2), and *gg*-E_3-*r* (TS2) kept the same *gg*-counterclockwise hydroxyl orientation during the ring conformation change. Given this conservation of the side chain conformation during ring distortion, the hydroxyl orientation of *gg*-$^4C_1$-*r* (IRC2) and *gg*-$B_{3,O}$-*r* (IRC2) differed from those of *tg*-$^4C_1$-*r* (OPT) and *gg*-$B_{3,O}$-*c* (OPT). This difference resulted in greater conformational energies for *gg*-$^4C_1$-*r* (IRC2) and *gg*-$B_{3,O}$-*r* (IRC2) compared to the optimized conformations. The energy differences for these conformers are shown in Figure 3. The energy of *gg*-$^4C_1$-*r* (IRC2) is 0.69 kcal/mol higher than that of *tg*-$^4C_1$-*r* (OPT), and the energy of *gg*-$B_{3,O}$-*r* (IRC2) is 2.61 kcal/mol higher than that of *gg*-$B_{3,O}$-*c* (OPT). The activation energy of the ring interconversion for the TS2 pathway is 5.61 kcal/mol. Although this energy is higher than that obtained for TS1, the difference is only 0.4 kcal/mol.

The ring-interconversion pathways for *tg*-$^4H_3$-*c* (TS3) and *gg*-$^2H_3$-*c* (TS4) were also investigated using IRC calculations. As the energies of the conformers at TS3 and TS4 are 2–3 kcal/mol higher than those of TS1 and TS2, the probability of ring interconversion via TS3 and TS4 is lower. However, it is important to clarify all the pathways for these four transition states because these states cover all four possible combinations (*tg*-*r*, *gg*-*r*, *tg*-*c*, and *gg*-*c*).

The IRC calculation showed that the terminal conformations of IRC3 and 4 toward the chair side were both $^4C_1$ ring conformations. However, the energies of *tg*-$^4C_1$-*c* (IRC3) and *gg*-$^4C_1$-*c* (IRC4) were greater than those of *tg*-$^4C_1$-*r* (OPT) because of the difference in the hydrogen-bond orientation pattern (Fig. 2m and o).

Table 2. Internal coordinates of the IRC terminal geometries calculated at the B3LYP/6-31G** for α-L-idopyranose

	IRC1		IRC2		IRC3		IRC4	
	tg-$^4C_1$-*r*	*tg*-$B_{3,O}$-*r*	*gg*-$^4C_1$-r	*gg*-$B_{3,O}$-*r*	*tg*-$^4C_1$-*c*	*tg*-$^1S_3$-*c*	*gg*-$^4C_1$-*c*	*gg*-$B_{3,O}$-*c*
Bond length (Å)								
C1–C2	1.528	1.547	1.526	1.544	1.529	1.541	1.525	1.539
C2–C3	1.520	1.520	1.518	1.520	1.525	1.523	1.522	1.520
C3–C4	1.527	1.523	1.529	1.522	1.527	1.526	1.530	1.529
C4–C5	1.544	1.558	1.547	1.559	1.543	1.556	1.551	1.564
C5–O5	1.439	1.441	1.436	1.439	1.428	1.438	1.434	1.444
O5–C1	1.421	1.413	1.424	1.410	1.438	1.421	1.430	1.426
O1–C1	1.397	1.410	1.398	1.413	1.388	1.409	1.387	1.403
O2–C2	1.419	1.427	1.420	1.427	1.416	1.421	1.415	1.417
O3–C3	1.422	1.421	1.424	1.421	1.419	1.418	1.421	1.418
O4–C4	1.426	1.428	1.429	1.431	1.423	1.424	1.426	1.425
O6–C6	1.415	1.412	1.421	1.411	1.434	1.435	1.432	1.431
C5–C6	1.541	1.535	1.540	1.531	1.538	1.527	1.537	1.524
Bond angle (deg)								
C1–C2–C3	108.5	109.3	108.2	109.1	109.6	109.8	108.3	109.2
C2–C3–C4	109.8	109.5	110.7	108.8	110.6	109.9	112.2	110.1
C3–C4–C5	111.6	110.1	113.2	109.9	110.1	108.6	112.6	109.8
C4–C5–O5	109.6	111.1	110.5	111.1	109.4	111.9	111.5	111.1
C5–O5–C1	116.7	116.3	116.5	117.0	117.9	116.0	119.4	116.9
O5–C1–C2	110.9	112.8	109.5	112.9	111.6	113.0	110.5	112.5
O1–C1–C2	107.0	107.0	107.0	107.0	108.5	107.4	109.1	108.0
O2–C2–C3	107.6	106.6	107.4	107.0	111.1	111.5	110.7	111.7
O3–C3–C4	106.8	107.0	106.3	107.1	111.0	111.9	110.8	111.1
O4–C4–C5	109.3	110.8	108.3	111.2	114.8	114.2	112.6	115.0
O6–C6–C5	111.0	112.1	115.3	113.6	107.4	107.1	115.5	109.9
C6–C5–O5	113.4	105.3	114.1	106.1	110.9	104.5	114.0	103.8
Dihedral angle (deg)								
C1–C2–C3–C4	−57.5	−58.0	−56.5	−60.1	−55.4	−44.9	−56.5	−61.5
C2–C3–C4–C5	55.0	56.2	49.7	57.0	57.2	64.6	49.6	52.4
C3–C4–C5–O5	−50.7	−2.6	−45.1	−3.2	−54.3	−22.7	−42.0	3.5
C1–O5–C5–C4	53.7	−53.3	52.2	−52.3	54.4	−38.6	47.2	−55.8
C2–C1–O5–C5	−58.4	51.8	−61.4	49.5	−53.9	59.9	−56.0	47.0
C3–C2–C1–O5	58.08	5.8	61.2	8.6	51.7	−14.4	57.4	12.6
H1–O1–C1–C2	178.8	−179.8	175.9	179.1	179.0	177.5	−175.8	172.9
H2–O2–C2–C3	178.5	−161.3	175.6	−162.1	−50.0	−53.6	−48.7	−49.3
H3–O3–C3–C4	−174.0	−174.0	−175.3	−171.9	45.4	47.4	48.6	46.8
H4–O4–C4–C5	167.8	169.7	176.0	167.8	28.9	−25.1	62.8	47.5
O6–C6–C5–O5	−158.9	−173.3	87.7	65.6	−171.7	−167.4	91.4	60.7
H6–O6–C6–C5	−57.6	−67.2	70.0	65.8	−175.7	−172.6	−76.1	−53.8
C6–C5–O5–C1	−75.5	−176.8	−77.4	−176.2	−73.8	−161.6	−83.2	−176.9

The IRC calculation toward the other side from TS3 and TS4 reached the *tg*-$^1S_3$-*c* (IRC3) and *gg*-$B_{3,O}$-*c* (IRC4) conformations. The conformation of *tg*-$^1S_3$-*c* (IRC3) was a new type obtained in our IRC calculations. A comparison of the hydroxyl orientations of *tg*-$^1S_3$-*c* (IRC3) and *tg*-$^1S_3$-*r* (OPT) showed that they have different patterns (Fig. 2d and n). Therefore, *tg*-$^1S_3$-*c* (IRC3) must again change its hydroxyl orientation to reach the optimized *tg*-$^1S_3$-*r* (OPT) conformation. In either case, however, the energies of *tg*-$^1S_3$-*r* (OPT) and *tg*-$^1S_3$-*c* (IRC3) were both found to be 3.8–4.2 kcal/mol higher than the lowest conformation. The conformation of $^1S_3$ might be an intermediate state to a more stable conformation, such as *gg*-$B_{3,O}$-*c* (OPT). In contrast, the energy of *gg*-$B_{3,O}$-*c* (IRC4) is only 0.40 kcal/mol higher than that of *gg*-$B_{3,O}$-*c* (OPT) and it has the same hydroxyl conformation type (Fig. 2c and p). Therefore, TS4 provides a direct pathway to the *gg*-$B_{3,O}$-*c* (OPT) conformation.

Ragazzi et al. postulated that interconversion from the $^4C_1$ chair to the skewed conformation occurs from $^4C_1$ to ^2S_O via $^2H_1$ with a transition barrier of 9.7 kcal/mol.[14] Stoddart presumed two possible pathways: one from $^4C_1$ to ^2S_O via $^2H_3$ and the other from $^4C_1$ to $^1S_3$ via $^4H_3$.[32] However, we found that the $^2H_3$ (TS4) transition state was on the interconversion path between $^4C_1$ and $B_{3,O}$ and that the transition energy was 7.86 kcal/mol. The comparison of transition states TS1 to TS4 and their ring-interconversion paths suggests that the most plausible ring-interconversion occurs between $^4C_1$ and $B_{3,O}$ via the E_3 envelope, which involves a 5.21 kcal/mol energy barrier.

As a summary of this section, it should be mentioned that the IRC terminal geometries in most cases do not match the OPT geometries as shown in Figure 3. In the case of $^4C_1$ ring conformation, the terminal geometries of IRC2–4 differ from $^4C_1$ (OPT) in their primary alcohol orientation and/or hydrogen-bond network pattern of hydroxyl residues. Similarly in the case of $B_{3,O}$ ring conformation, the terminal geometries of IRC1 and IRC2 differ from $B_{3,O}$ (OPT). The ring transition states mainly attribute to only the ring vibration mode, which is not related to the vibration of the hydroxyl residue. Therefore, in the case that the geometries obtained were different in IRC and OPT, we proposed the two-step process discussed above. That is, the transition of the ring conformation occurs first, and then the hydroxyl residue orientation would occur toward the lower energy conformations. In this work, we focused on obtaining the TS geometries of the ring interconversion and their paths. Further studies are needed to clarify the whole process proposed here.

3.3. Conformations along the IRC pathway

In order to trace the conformational change along the interconversion path via transition states, the conformations were investigated using the IRC calculation. The conformations obtained are represented using Cremer–Pople ring puckering parameters and are shown in Figure 4. The values of the Cremer–Pople ring puckering parameters for the key geometries shown in Tables 1 and 2 are listed in Table 3. Note that each conformational change occurs without a large deviation in the ϕ value on this map. As the value ϕ is the phase angle and represents the twisting of the ring plane, such as the boat and skewed conformations, this shows that ring interconversion proceeded without involving some boat and skewed conformations. Each transition state exists at the midpoint along the route of its conformational change. To investigate the conformational changes for these pathways more precisely, the changes in the bond and dihedral angles of the pyranose ring along the interconversion paths were analyzed and are shown in Figure 5. For all paths, the C5–O5–C1 bond angle changed the most compared to the other angles. For the dihedral angles, while the C1–C2–C3–C4 and C2–C3–C4–C5 dihedral angles did not change, the C4–C5–O5–C1 and C5–O5–C1–C2 angles changed markedly in tandem. The C3–C4–C5–O5 and O5–C1–C2–C3 dihedral angles also changed in tandem. The behavior of the bond and dihedral angles was similar in all paths. These results indicate that only the ring oxygen atom causes the large changes in the bond and dihedral angles. This corresponds to the fact that the ring oxygen atom had a large amplitude of the imaginary frequency at the transition state.

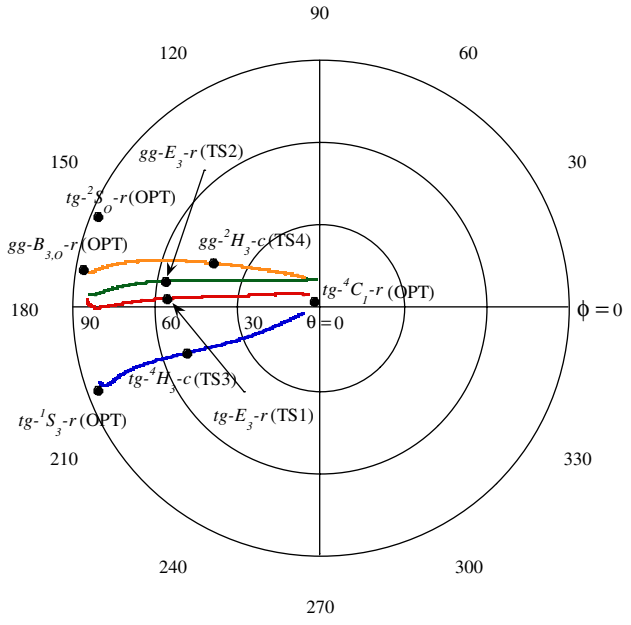

Figure 4. The interconversion paths expressed using the Cremer–Pople ring puckering parameters. Red line: the path connecting *tg*-$^4C_1$-*r* (IRC1) and *tg*-$B_{3,O}$-*r* (IRC1) via *tg*-E_3-*r* (TS1). Green line: the path connecting *gg*-$^4C_1$-*r* (IRC2) and *gg*-$B_{3,O}$-*r* (IRC2) via *gg*-E_3-*r* (TS2). Blue line: the path connecting *tg*-$^4C_1$-*c* (IRC3) and *tg*-$^1S_3$-*c* (IRC3) via *tg*-$^4H_3$-*c* (TS3). Orange line: the path connecting *gg*-$^4C_1$-*c* (IRC4) and *gg*-$B_{3,O}$-*c* (IRC4) via *gg*-$^2H_3$-*c* (TS4). The optimized conformations and transition-state conformations are shown as solid circles.

Table 3. Cremer–Pople puckering parameters (Θ and ϕ) of the optimized, TS, and IRC terminal geometries calculated at the B3LYP/6-31G** for α-L-idopyranose

		Puckering parameters	
		Θ	ϕ
OPT	*tg*-$^4C_1$-*r* (OPT)	3.05	129.77
	tg-^2S_O-*r* (OPT)	87.21	157.84
	gg-$B_{3,O}$-*c* (OPT)	87.19	171.03
	tg-$^1S_3$-*r* (OPT)	86.24	200.53
TS1	*tg*-$^4C_1$-*r* (IRC1)	6.21	134.69
	tg-E_3-*r* (TS1)	55.87	176.72
	tg-$B_{3,O}$-*r* (IRC1)	84.94	177.91
TS2	*gg*-$^4C_1$-*r* (IRC2)	10.52	98.27
	gg-E_3-*r* (TS2)	57.18	170.33
	gg-$B_{3,O}$-*r* (IRC2)	83.62	176.79
TS3	*tg*-$^4C_1$-*c* (IRC3)	6.15	199.16
	tg-$^4H_3$-*c* (TS3)	51.45	198.89
	tg-$^1S_3$-*c* (IRC3)	84.77	198.76
TS4	*gg*-$^4C_1$-*c* (IRC4)	12.09	117.05
	gg-$^2H_3$-*c* (TS4)	41.99	157.46
	gg-$B_{3,O}$-*c* (IRC4)	84.82	171.50

4. Conclusions

In summary, the most plausible ring interconversion of the α-L-idopyranose ring occurs between $^4C_1$ and $B_{3,O}$ via the E_3 envelope, which involves a 5.21 kcal/mol

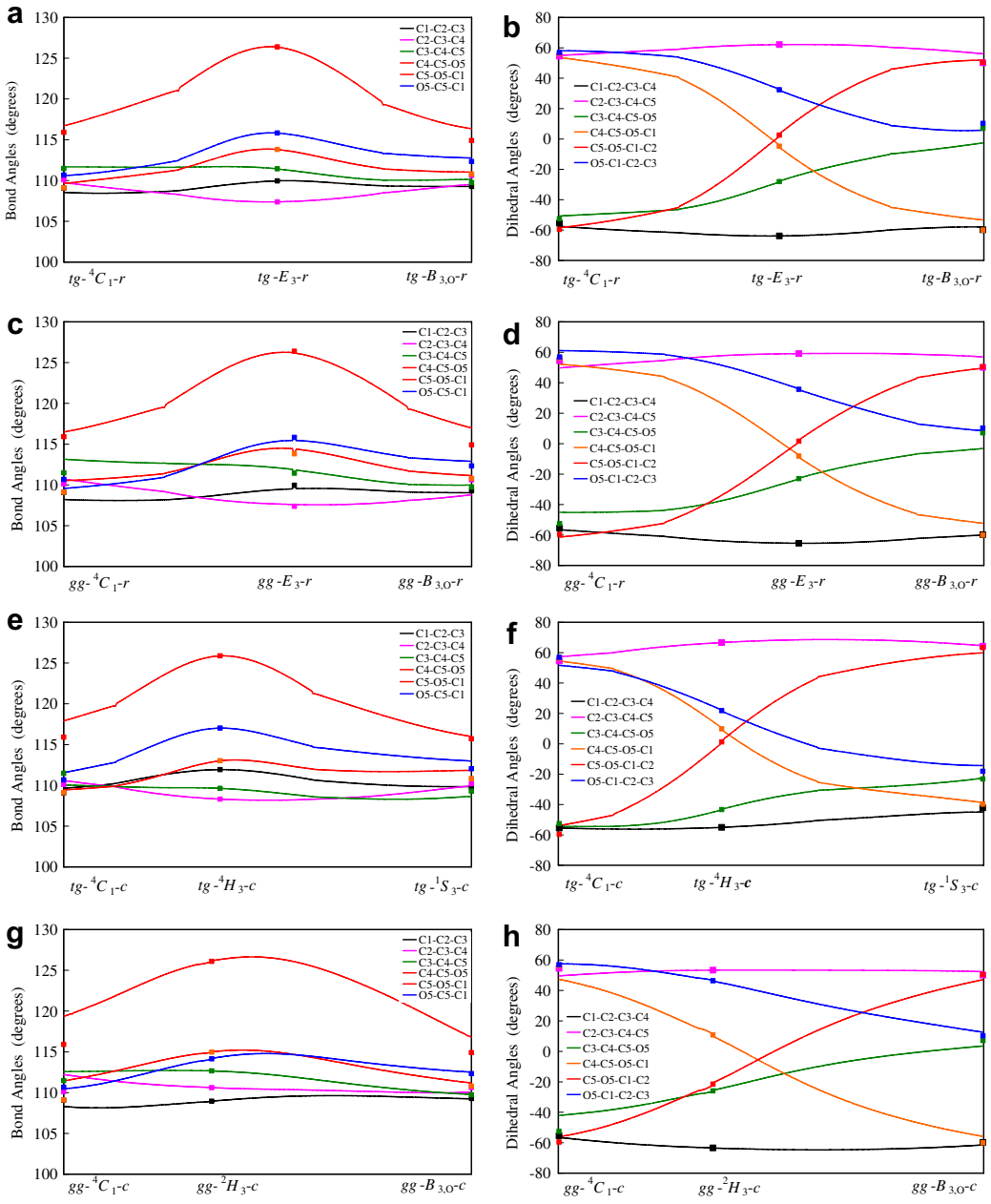

Figure 5. The change in the bond and dihedral angles along the four ring interconversion paths. The squares indicate the values for the optimized conformations at *tg*-$^4C_1$-*r* (OPT), the transition states, and the optimized *gg*-$B_{3,O}$-*c* (OPT) or *tg*-$^1S_3$-*r* (OPT) conformations from the left in each figure. (a) Bond angle change along the path via TS1, (b) dihedral angle change along the path via TS1, (c) bond angle change along the path via TS2, (d) dihedral angle change along the path via TS2, (e) bond angle change along the path via TS3, (f) dihedral angle change along the path via TS3, (g) bond angle change along the path via TS4, and (h) dihedral angle change along the path via TS4.

energy barrier. In the frequency analysis of the transition-state conformations, the ring oxygen atom showed a large amplitude in the imaginary frequency. Ernst et al. pointed out that the energy barrier of an interconversion path will be lowest if the endocyclic dihedral angle involves the unsubstituted ring oxygen.[17] When only the ring oxygen atom moves upward and downward with respect to the ring plane from the E_3 conformation, its movement will result in $^4C_1$ and $B_{3,O}$, respectively. This also supports the ring-interconversion pathway from $^4C_1$ to $B_{3,O}$ via the E_3 envelope conformation, which was proposed as the most plausible path in this study. The energy difference between *tg*-E_3-*r* (TS1) and *gg*-E_3-*r* (TS2) was only 0.40 kcal/mol, and that between *tg*-$B_{3,O}$-*r* (IRC1) and *gg*-$B_{3,O}$-*r* (IRC2) was only 0.87 kcal/mol. Although the hydroxyl residue orientations differed in these two states, TS1 and TS2 would both be actual transition states for this molecule. The transition-state structure would be important for parameterizing the molecular dynamics in order to

express the flexibility of the pyranose ring of carbohydrates and their derivatives.

Acknowledgements

This work was supported by a Grant-in-Aid (No. 17300093) from the Ministry of Education, Culture, Sports, Science, and Technology of Japan. The authors also thank Professor John Brady at Cornell University for helpful discussions.

References

1. Rudrum, M.; Shaw, D. F. *J. Chem. Soc.* **1965**, 52–57.
2. Angyal, S. J. *Angew. Chem., Int. Ed. Engl.* **1969**, *8*, 157–166.
3. Angyal, S. J.; Pickles, V. A. *Aust. J. Chem.* **1972**, *25*, 1695–1710.
4. Snyder, J. R.; Serianni, A. S. *J. Org. Chem.* **1986**, *51*, 2694–2702.
5. Ferro, D. R.; Provasoli, A.; Ragazzi, M.; Torri, G.; Casu, B.; Gatti, G.; Jacquinet, J.-H.; Sinaÿ, P.; Petitou, M.; Choay, J. *J. Am. Chem. Soc.* **1986**, *108*, 6773–6778.
6. Sanderson, P. N.; Huckerby, T. N.; Nieduszynski, I. A. *Biochem. J.* **1987**, *243*, 175–181.
7. Ferro, D. R.; Provasoli, A.; Ragazzi, M.; Casu, B.; Torri, G.; Bossennec, V.; Perly, B.; Sinaÿ, P.; Petitou, M.; Choay, J. *Carbohydr. Res.* **1990**, *195*, 157–167.
8. Mikhailov, D.; Mayo, K. H.; Vlahov, I. R.; Toida, T.; Pervin, A.; Linhardt, R. J. *Biochem. J.* **1996**, *318*, 93–102.
9. Mikhailov, D.; Linhardt, R. J.; Mayo, K. H. *Biochem. J.* **1997**, *328*, 51–61.
10. Mulloy, B.; Forster, M. J. *Glycobiology* **2000**, *10*, 1147–1156.
11. Atkins, E. D. T.; Isaac, D. H. *J. Mol. Biol.* **1973**, *80*, 773–779.
12. Mitra, A. K.; Arnott, S.; Atkins, E. D. T.; Isaac, D. H. *J. Mol. Biol.* **1983**, *169*, 873–901.
13. Faham, S.; Hileman, R. E.; Fromm, J. R.; Linhardt, R. J.; Rees, D. C. *Science* **1996**, *271*, 1116–1120.
14. Ragazzi, M.; Ferro, D. R.; Provasoli, A. *J. Comput. Chem.* **1986**, *7*, 105–112.
15. Forster, M. J.; Mulloy, B. *Biopolymers* **1993**, *33*, 575–588.
16. Dowd, M. K.; French, A. D.; Reilly, P. J. *Carbohydr. Res.* **1994**, *264*, 1–19.
17. Ernst, S.; Venkataraman, G.; Sasisekharan, V.; Langer, R.; Cooney, C. L.; Sasisekharan, R. *J. Am. Chem. Soc.* **1998**, *120*, 2099–2107.
18. Angulo, J.; Nieto, P. M.; Martín-Lomas, M. *Chem. Commun. (Cambridge)* **2003**, 1512–1513.
19. Verli, H.; Guimarães, J. A. *Carbohydr. Res.* **2004**, *339*, 281–290.
20. Ma, B.; Schaefer, H. F., III; Allinger, N. L. *J. Am. Chem. Soc.* **1998**, *120*, 3411–3422.
21. Csonka, G. I. *J. Mol. Struct. (THEOCHEM)* **2002**, *584*, 1–4.
22. Momany, F. A.; Willett, J. L. *J. Comput. Chem.* **2000**, *21*, 1204–1219.
23. Casu, B.; Petitou, M.; Provasoli, M.; Sinaÿ, P. *Trends Biochem. Sci.* **1998**, *13*, 221–225.
24. Venkataraman, G.; Sasisekharan, V.; Cooney, C. L.; Langer, R.; Sasisekharan, R. *Proc. Natl. Acad. Sci. U.S.A.* **1994**, *91*, 6171–6175.
25. Cremer, D.; Pople, J. A. *J. Am. Chem. Soc.* **1975**, *97*, 1354–1358.
26. Ionescu, A. R.; Bérces, A.; Zgierski, M. Z.; Whitfield, D. M.; Nukada, T. *J. Phys. Chem. A* **2005**, *109*, 8096–8105.
27. Novoa, J. J.; Sosa, C. *J. Phys. Chem.* **1995**, *99*, 15837–15845.
28. Csonka, G. I.; Éliás, K.; Csizmadia, I. G. *Chem. Phys. Lett.* **1996**, *257*, 49–60.
29. Frisch, M. J.; Trucks, G. W.; Schlegel, H. B.; Scuseria, G. E.; Robb, M. A.; Cheeseman, J. R.; Montgomery, J. A., Jr.; Vreven, T.; Kudin, K. N.; Burant, J. C.; Millam, J. M.; Iyengar, S. S.; Tomasi, J.; Barone, V.; Mennucci, B.; Cossi, M.; Scalmani, G.; Rega, N.; Petersson, G. A.; Nakatsuji, H.; Hada, M.; Ehara, M.; Toyota, K.; Fukuda, R.; Hasegawa, J.; Ishida, M.; Nakajima, T.; Honda, Y.; Kitao, O.; Nakai, H.; Klene, M.; Li, X.; Knox, J. E.; Hratchian, H. P.; Cross, J. B.; Bakken, V.; Adamo, C.; Jaramillo, J.; Gomperts, R.; Stratmann, R. E.; Yazyev, O.; Austin, A. J.; Cammi, R.; Pomelli, C.; Ochterski, J. W.; Ayala, P. Y.; Morokuma, K.; Voth, G. A.; Salvador, P.; Dannenberg, J. J.; Zakrzewski, V. G.; Dapprich, S.; Daniels, A. D.; Strain, M. C.; Farkas, O.; Malick, D. K.; Rabuck, A. D.; Raghavachari, K.; Foresman, J. B.; Ortiz, J. V.; Cui, Q.; Baboul, A. G.; Clifford, S.; Cioslowski, J.; Stefanov, B. B.; Liu, G.; Liashenko, A.; Piskorz, P.; Komaromi, I.; Martin, R. L.; Fox, D. J.; Keith, T.; Al-Laham, M. A.; Peng, C. Y.; Nanayakkara, A.; Challacombe, M.; Gill, P. M. W.; Johnson, B.; Chen, W.; Wong, M. W.; Gonzalez, C.; Pople, J. A. *Gaussian 03, Revision B.04*; Gaussian: Pittsburgh, PA, 2003.
30. Nishida, Y.; Ohrui, H.; Meguro, H. *Tetrahedron Lett.* **1984**, *25*, 1575–1578.
31. Brady, J. W.; Schmidt, R. K. *J. Phys. Chem.* **1993**, *97*, 958–966.
32. Stoddart, J. F. *Stereochemistry of Carbohydrates*; Wiley: New York, 1971; pp 57–58.